Scattering of spinon excitations by potentials in the one-dimensional Heisenberg model

A. Pavlis[1,2] and X. Zotos[1,2,3]

[1]*ITCP and CCQCN, Department of Physics, University of Crete, 71003 Herakleio, Greece*

[2]*Foundation for Research and Technology-Hellas, 70013 Herakleio, Greece*

[3]*Leibniz Institute for Solid State and Materials Research Dresden, 01069 Dresden, Germany*

(Received 11 January 2019; revised manuscript received 3 July 2019; published 1 October 2019)

By a semianalytical Bethe ansatz method and a T-matrix approach we study the scattering of a spinon, the elementary quantum many-body topological excitation in the one-dimensional (1D) Heisenberg model, by local and phonon potentials. In particular, we contrast the scattering of a spinon to that of a free spinless fermion in the XY model to highlight the effect of strong correlations. For the one-spinon scattering in an odd-site chain, we find regular behavior of the scattering coefficients. In contrast, in an even-site chain there is a transfer of transmission probability between the two spinon branches that grows exponentially with system size. We link the exponent of the exponential behavior to the dressed charge that characterizes the critical properties of the 1D Heisenberg model, an interplay of topological and critical properties. The aim of this study is a microscopic understanding of spinon scattering by impurities, barriers, or phonons, modeled as prototype potentials, an input in the analysis of quantum spin transport experiments.

DOI: 10.1103/PhysRevB.100.134401

I. INTRODUCTION

The novel mode of thermal transport by magnetic excitations in quasi-one-dimensional quantum magnets has been, over the last few years, the focus of extensive experimental [1] and theoretical studies [2–7]. It was promoted by the fortuitous coincidence of synthesis of excellent-quality compounds very well described by prototype integrable spin chain models and the proposal of unconventional (ballistic) spin and thermal transport in these systems [2]. Of course, the purely ballistic thermal transport predicted by theory is not observed in thermal conduction experiments as the, albeit very high, thermal conductivity is limited by the scattering of the magnetic excitations from impurities and phonons [1].

In parallel, in the field of spintronics (spin caloritronics) there is renewed interest in the transport of magnetization, with the (inverse) spin Hall and spin Seebeck effects employed for the generation and detection of spin currents [8,9]. So far mostly metallic, semiconducting, and magnetically ordered (ferro-, antiferro-, ferri-) magnetic materials have been studied. Only very recently was the spin Seebeck effect studied in the quasi-one-dimensional quantum magnet Sr_2CuO_3 accurately described by a spin-1/2 Heisenberg chain [10].

Regarding quasi-one-dimensional quantum magnets, a lot is known about their bulk thermodynamic [11] and magnetothermal transport properties [12–14]. The prototype model for these systems is the well-studied one-dimensional (1D) Heisenberg model that is analytically solvable by the Bethe ansatz (BA) method. The elementary excitations in this strongly correlated system are topological in nature (the spinons [15]), and most of thermodynamic and transport experiments are discussed in terms of these low-energy excitations [1,4,6].

In this work, we study the scattering of a spinon from local potentials, aiming at a microscopic understanding of scattering processes by impurities, phonons, and barriers, which is relevant to (far out of equilibrium) quantum spin transport. At the moment, we do not address any particular experiment; we only present background work on the theoretical question of how a quantum many-body topological excitation scatters from a potential. This question is also relevant in other systems with topological excitations of actual experimental and theoretical interest.

To this end, we first use a recently developed semianalytical Bethe ansatz method [16,17] to evaluate scattering matrix elements by prototype potentials and then to evaluate scattering coefficients by a T-matrix method. We should emphasize that although it is an elementary exercise to evaluate the quantum mechanical scattering coefficients (reflection, transmission) of a free particle from a potential barrier, little is known on the scattering of a quantum many-body quasiparticle excitation, even less for a topological one. The Bethe-ansatz-solvable models offer exactly such a framework for the study of this fundamental problem.

II. MODEL AND MATRIX ELEMENTS

The XXZ anisotropic Heisenberg Hamiltonian for a chain of N sites with periodic boundary conditions $S^a_{N+1} = S^a_1$ and in the presence of a local potential V of strength g is given by

$$H = \sum_{n=1}^{N} h_{n,n+1} + gV,$$
$$h_{n,n+1} = J\left(S^x_n S^x_{n+1} + S^y_n S^y_{n+1} + \Delta S^z_n S^z_{n+1} - hS^z_n\right), \qquad (1)$$

where $S^a_n = \frac{1}{2}\sigma^a_n$, σ^a_n are Pauli spin operators with components $a = x, y, z$ at site n, h is the magnetic field, and the anisotropy parameter Δ is typically parametrized as $\Delta = \cos\gamma$. In the following we will focus on the easy-plane antiferromagnet, $0 \leqslant \Delta \leqslant 1$, and we will take $J = 1$ as the unit of energy.

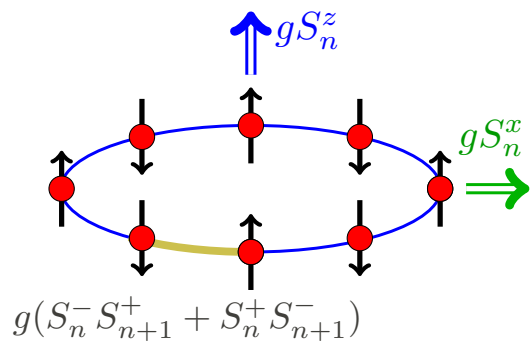

FIG. 1. Schematic of the spin chain and the type of potentials in consideration.

We study chains with odd and even numbers N of spins. In odd chains, for each total $S^z = \pm 1/2$, the ground state is doubly degenerate, containing one spinon with dispersion given by the one-branch $\varepsilon_Q = v_s|\sin Q|, \quad 0 < Q < \pi$. For even N the lowest excitations involve at least two spinons, with the dispersion of each spinon given by $\varepsilon_Q = v_s|\sin Q|$, i.e., states of the Cloizeaux-Pearson spinon spectrum [15,18]. We will study states belonging to the lowest-energy branch of the $M = N/2 - 1$ magnetization sector obtained from the $S^z = 1$ states by keeping the one-spinon momentum fixed at zero and considering the dispersion of the second. In the spinon dispersion, $v_s = \frac{\pi}{2}\frac{\sin\gamma}{\gamma}$, and Q is defined as the spinon momentum above the ground state. Normalized spinon states $|Q\rangle = |\{\lambda\}\rangle$ are determined from a specific set of Bethe roots $\{\lambda_j\}_{j=1}^M$ (see the Supplemental Material [19] and also references therein), and matrix elements between such states describe spinon scattering processes. Moreover, we define the spinon group velocity as $u_Q = d\varepsilon_Q/dQ$.

In the following we first evaluate scattering matrix elements $|\mathcal{M}|^2 = |\langle Q'|V|Q\rangle|^2$ of a spinon from a state of momentum Q to a state of momentum Q' on finite-size lattices following [16,17,19]. We show in particular that they are strongly enhanced compared to those of single-particle excitations, leading to unusual scattering coefficients. The potentials we consider are schematically shown in Fig. 1.

To start with we consider a one-site longitudinal potential $V = S_n^z$ at site n. The corresponding matrix element is given by [20]

$$\left|\mathcal{M}_q^z(Q)\right|^2 = \left|\langle Q+q|S_q^z|Q\rangle\right|^2, \tag{2}$$

where $S_n^z = \frac{1}{\sqrt{N}}\sum_q e^{-iqn}S_q^z$. In the simple $\Delta = 0$ case, the XY model, by a Jordan-Wigner transformation the spectrum corresponds to that of free spinless fermions, $|M_q^z|^2 = 1/N$, and the potential moves only one fermion to a different state [21].

In sharp contrast, in the isotropic Heisenberg model ($\Delta = 1$), due to strong antiferromagnetic fluctuations, the scattering matrix elements are drastically enhanced, as shown in Fig. 2. $|\mathcal{M}_q^z(Q=0)|^2$ scales overall as $1/\sqrt{N}$, and as indicated in the inset of Fig. 2, in the region not close to $q = 0, \pi$, the matrix element behaves approximately as

$$\left|\mathcal{M}_q^z(Q=0)\right|^2 \sim \frac{1}{\sqrt{N}}\frac{1}{(\pi-q)^{2/3}}. \tag{3}$$

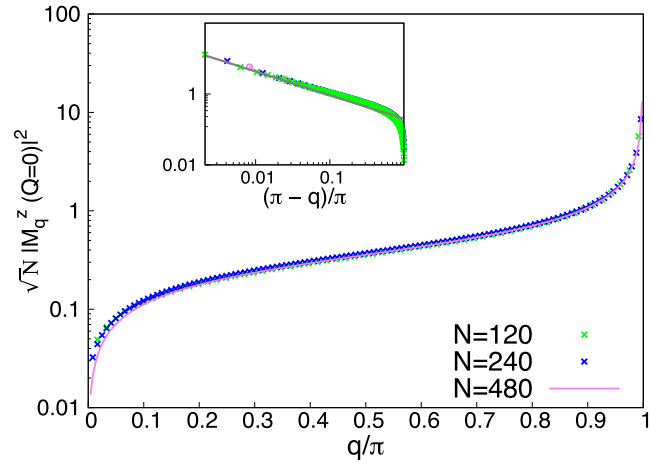

FIG. 2. Scaled $\sqrt{N}|\mathcal{M}_q^z(Q=0)|^2$ as a function of q/π for $N = 120, 240, 360, 480$, $\Delta = 1$. The inset shows the asymptotic scaling of $|\mathcal{M}_q^z(Q=0)|^2$, with the solid line indicating the asymptote $(\pi - q)^{2/3}$.

Note that this behavior does not describe $q = \pi$, which should not be diverging and scales differently with N, as will be discussed below.

The most interesting part in Fig. 2 and relation (3) is that the matrix elements scale in a nontrivial fashion with N. In the XY model and for an S_n^z potential all matrix elements scale as $1/N$, which is the usual case in lattice scattering. On the contrary, for all $\Delta \neq 0$ the matrix elements have a nontrivial relation with respect to the spinon momentum and a particular scaling with respect to the number of spin sites, which is crucial to the spinon scattering.

Furthermore, using [16] and a numerical evaluation, we further address the two types of matrix elements shown in Fig. 3 (and all equivalent transitions between the two spinon branches), and as we will see in the next section, they play a significant role in the scattering processes. In the $q = \pi$ transition

$$\left|\langle Q+\pi|S_\pi^z|Q\rangle\right|^2 \simeq \frac{f^z(Q)}{N^{2Z^z-1}}, \tag{4}$$

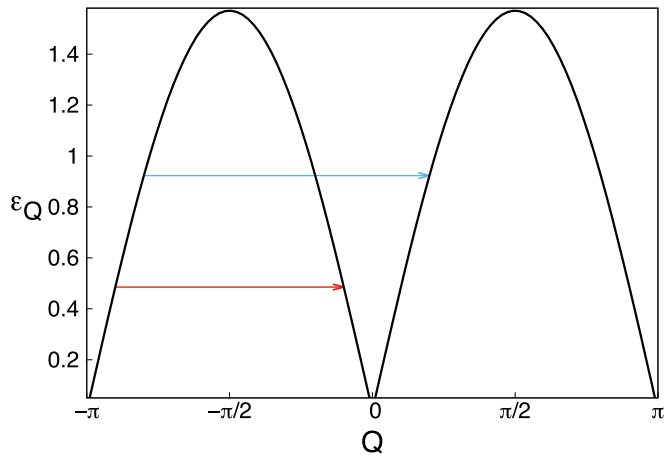

FIG. 3. Schematic description of the $Q \to \pi + Q$ transition (blue arrow) and $Q \to \pi - Q$ same-branch velocity-flipping transition (red arrow).

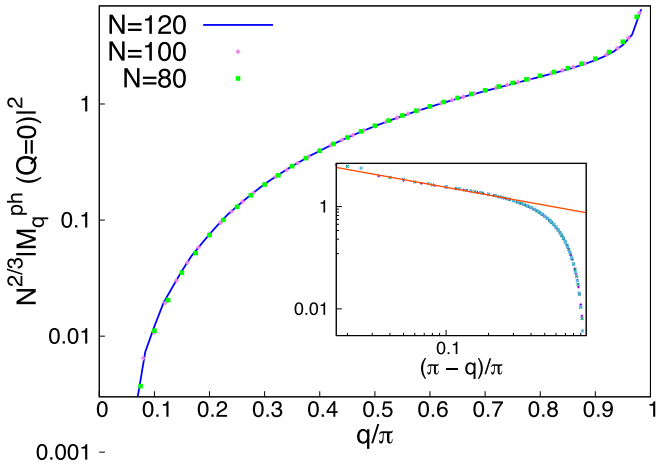

FIG. 4. Scaled $N^{\frac{2}{3}}|\mathcal{M}_q^{ph}(Q=0)|^2$ as a function of q/π. The inset shows the asymptotic scaling of $|\mathcal{M}_q^{ph}(Q=0)|^2$ as a function of $(\pi-q)/\pi$. The solid line indicates the asymptote $(\pi-q)^{1/2}$.

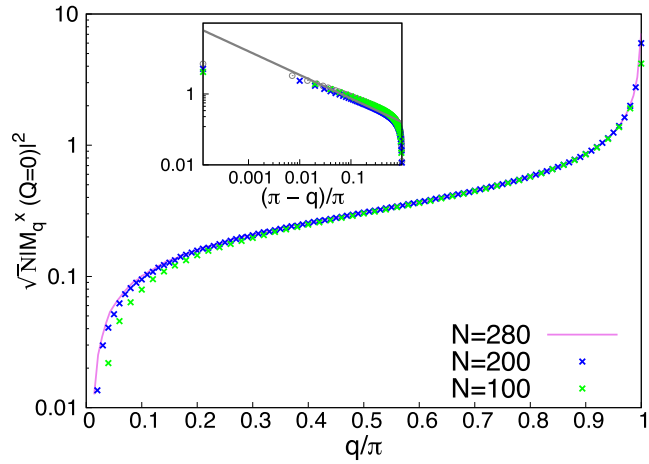

FIG. 5. Scaled $|M_q^x(Q=0)|^2\sqrt{N}$ vs q for the isotropic model $\Delta=1$ and various N. The solid line in the inset shows that the asymptote scales as $(\pi-q)^{2/3}$.

and in the same-branch velocity-flipping transition

$$\left|\langle\pi-Q|S^z_{\pi-2Q}|Q\rangle\right|^2 \simeq \frac{h^z(Q)}{N^{\alpha(Q)}}, \tag{5}$$

both corresponding to on-shell transitions. $\mathcal{Z}$ is the dressed charge introduced in [22,23], and the identification has been done using the analysis in [24] since for small magnetic fields the dressed charge is $\mathcal{Z}\simeq\sqrt{\frac{\pi}{2(\pi-\gamma)}}$. In particular, $\mathcal{Z}^2=1$ for $\Delta=0$, and $\mathcal{Z}^2=1/2$ for $\Delta=1$. Note that this scaling of the matrix elements is also valid in the $h=0$ case since by an analytical continuation the critical exponent $2\mathcal{Z}^2$ remains the same. Furthermore, for Q not close to zero $\alpha(Q)\simeq 1$, and $f^z(Q)$ is an almost constant function, while $h^z(Q)$ is a rapidly decreasing one to a constant value [19]. These types of matrix elements were extensively studied in [25,26], and the correspondence between the dressed charge and the scaling of the matrix elements has been proven analytically.

Next, we consider the scattering of a spinon by a lattice distortion of wave vector q,

$$h_q=\frac{1}{\sqrt{N}}\sum_{n=1}^{N}e^{iqn}J\left(S^x_nS^x_{n+1}+S^y_nS^y_{n+1}\right), \tag{6}$$

from which we can deduce the scattering from a "weak link" $V=g(S^-_nS^+_{n+1}+S^+_nS^-_{n+1})$. Similar to the previous case, the scaled scattering matrix element for $\Delta=1$ and the asymptotic form

$$\left|\mathcal{M}_q^{ph}(Q=0)\right|^2\sim N^{-2/3}\frac{1}{(\pi-q)^{1/2}} \tag{7}$$

for $Q=0$ are shown in Fig. 4.

Again, the dominant matrix elements for spinon scattering are a π transition and a same-branch velocity-flipping matrix element,

$$|\langle Q+\pi|h_\pi|Q\rangle|^2\simeq\frac{f^{ph}(Q)}{N^{a(Q)}},$$
$$|\langle\pi-Q|h_{\pi-2Q}|Q\rangle|^2\simeq\frac{h^{ph}(Q)}{N}. \tag{8}$$

For the isotropic $\Delta=1$ case, $a(Q)$ has a weak dependence with respect to Q, $a(Q)\simeq 0.4$ around $Q=2\pi/10$, while by a Jordan-Wigner transformation we can derive that for $\Delta=0$ the absolute value squared of all matrix elements scales as $1/N$.

Finally, we consider a transverse magnetic potential, $V=gS^x_n$. The main difference of this potential from the two previous ones is that it acts nontrivially only between states with $\Delta S^z=\pm1$.

Similar to the S^z_n potential, as shown in Fig. 5, the asymptote behaves as

$$\left|M_q^x(Q=0)\right|^2\sim\frac{1}{\sqrt{N}}\frac{1}{(\pi-q)^{2/3}}, \tag{9}$$

and the dominant matrix elements scale as

$$\left|\langle Q+\pi|S^x_\pi|Q\rangle\right|^2\simeq\frac{f^x(Q)}{N^{\frac{1}{2\mathcal{Z}^2}-1}}. \tag{10}$$

This time, the XY model matrix elements behave nontrivially as they scale as $\sqrt{N}$, and in fact, they imply the strongest scattering compared to the $0<\Delta\leqslant 1$ case.

Overall, the π transitions show a strong N dependence and a weak Q dependence, while the $\pi-2Q$ (velocity flip) transitions show a $1/N$ dependence and a strong Q dependence [19].

To close our discussion on the matrix elements, we consider an extended potential profile $V_{\text{ext}}=\sum_{n=1}^{N}g_nV_n$, where V_n represents one of the potentials we studied above and g_n is the potential profile,

$$|\langle Q+q|V_{\text{ext}}|Q\rangle|^2=\frac{1}{N}\left|\sum_{n=1}^{N}g_ne^{-iqn}|^2\right|V_q|^2. \tag{11}$$

For example, for a segment of m sites with a potential $V_m=\sum_{n=N/2}^{N/2+m-1}S^z_n$ the matrix element is given by

$$|\langle Q+q|V_m|Q\rangle|^2=\frac{1}{N}\frac{\sin^2\frac{qm}{2}}{\sin^2\frac{q}{2}}\left|\mathcal{M}_q^z(Q)\right|^2. \tag{12}$$

This form of equation can be interpreted as a "diffraction"-like pattern modified by the scattering of the spinon. For the XY

model it simply becomes

$$|\langle Q+q|V_m|Q\rangle|^2 = \frac{1}{N^2}\frac{\sin^2\frac{qm}{2}}{\sin^2\frac{q}{2}}. \tag{13}$$

The main message of this section is that the scattering matrix elements of the quantum many-body topological (spinon) excitations in the XXZ Heisenberg model are strongly enhanced compared to the ones in the XY model (free fermions). They show a nontrivial system size dependence, and thus, we expect profound differences in the scattering of spinon excitations by a potential from the generic single-particle one.

III. SCATTERING COEFFICIENTS

We will analyze the transmission and reflection scattering coefficients of a spinon from a potential within the T-matrix approach (see the Supplemental Material [19] and also reference therein) by writing all quantities in the basis of Bethe ansatz eigenstates $|\{\lambda\}\rangle$,

$$\begin{aligned} T &= V\frac{1}{1-G_0V}, \\ G_0(E) &= \lim_{\varepsilon\to 0}\sum_{\{\lambda\}}\frac{|\{\lambda\}\rangle\langle\{\lambda\}|}{E-E_{\{\lambda\}}+i\varepsilon}, \\ V &= \sum_{\{\mu\},\{\lambda\}}\langle\{\lambda\}|V|\{\mu\}\rangle|\{\lambda\}\rangle\langle\{\mu\}|. \end{aligned} \tag{14}$$

$E_{\{\lambda\}}$ is the energy corresponding to the Bethe state $|\{\lambda\}\rangle$. Based on the discussion in the previous section for the particular scaling of the matrix elements with N, we write a typical matrix element in the form $\langle\{\lambda\}|V|\{\mu\}\rangle = gf_{\{\lambda\},\{\mu\}}/N^\alpha$, with g being the potential strength and $\alpha = \alpha(\{\lambda\},\{\mu\}) > 0$ being a scaling factor. The potential matrix V belongs in a Hilbert space of dimension $\dim\mathcal{H} = 2^N$, which makes the problem intractable from a computational point of view. Therefore, in order to be able to calculate the scattering coefficients for relatively long spin chains, we restrict our numerical calculations to including only the two-spinon continuum, i.e., a subspace of dimension $\dim\mathcal{H}_{2sp} = \frac{N}{8}(N+2)$. The calculation of the T matrix is straightforward; we compute the matrix $1-G_0V$ and subsequently invert it and left multiply it by V. Note that for the evaluation of the Green's function G_0 we use the identity $\lim_{\varepsilon\to 0}\frac{1}{x+i\varepsilon} = P\frac{1}{x} - i\pi\delta(x)$, where P stands for the Cauchy principal value part.

A. "Free" spinon

It is instructive to consider the scattering of a free particle on a lattice with the "spinon" dispersion relation $\varepsilon_Q = v_s|\sin Q|$ by a one-site δ-like potential of strength g. In this case all the matrix elements are the same, $\langle Q'|V|Q\rangle = g/N$, and the transmission coefficient $\mathcal{T}_{Q,Q}$ is a function of g/u_Q [19], $u_Q = d\varepsilon_Q/dQ$.

In Fig. 6 we show that the "free"-spinon transmission probability and that of a particle in a tight-binding model with the dispersion relation $\varepsilon_Q = v_s(1-\cos Q)$ behave very differently. The free-spinon transmission probability is generally a decreasing function of the energy, a property of the specific bounded spectrum. Moreover, we observe that in the linear part of the energy dispersion we have high transmission probability, which is related to the fact that in a purely linear dispersion relation, i.e., a massless one-dimensional Dirac equation, only a phase is induced in the wave function and there is no reflection probability [27]. Additionally, from the specific form of the spinon dispersion relation we observe that when ε_Q decreases, u_Q increases, which implies that $\mathcal{T}_{Q,Q}$ is an increasing function of the spinon velocity. Thus, a more sensible quantity for the description of the transmission coefficient is the spinon velocity and not the spinon energy as in usual scattering problems.

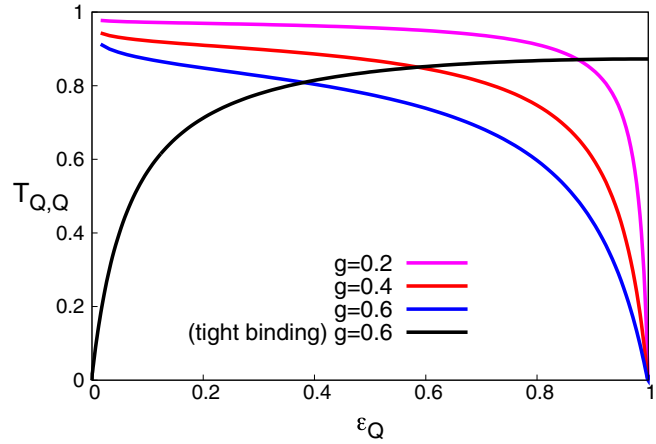

FIG. 6. $\mathcal{T}_{Q,Q}$ vs ε_Q for the scattering of a "free" particle and a particle in a tight-binding model from a δ-like potential of strength g.

B. One-site longitudinal potential

We first consider the scattering of a spinon in an odd-site chain from a one-site potential $V = gS^z_n$. In the fermionic language of the $t-V$ model [28] this would, indeed, correspond to the scattering of a spinless fermion from a one-site potential. In our calculation of the transmission coefficient $\mathcal{T}_{Q,Q}$ as a function of spinon energy (Fig. 7), we include only the lower one-spinon branch as intermediate states. For $\Delta = 0$

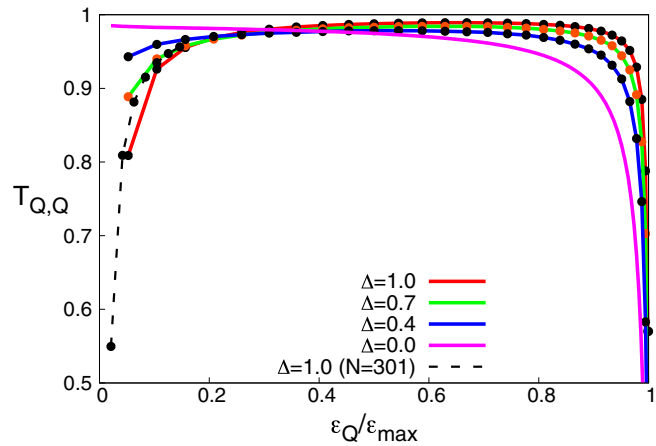

FIG. 7. $\mathcal{T}_{Q,Q}$ vs ε_Q for various Δ, $g = 0.15$ for an odd spin chain, $N = 121$. The black dashed line indicates the $N = 301$ data. The solid lines are guides to the eye.

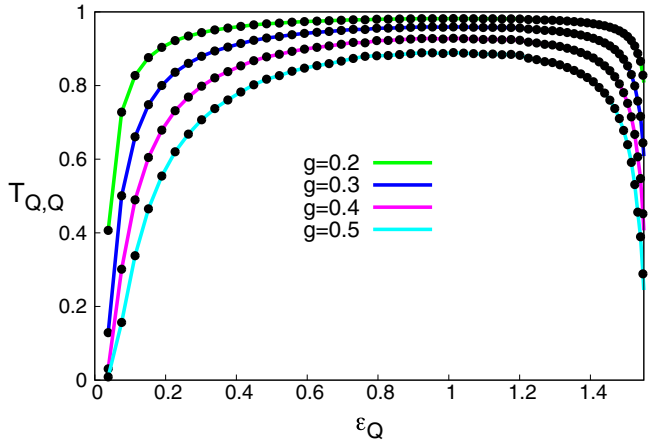

FIG. 8. $\mathcal{T}_{Q,Q}$ vs ε_Q for an odd $N = 241$ isotropic model spin chain for various g. The solid lines are guides to the eye.

we recover the free-spinon result of Fig. 6, while for finite Δ we find strong suppression of the transmission probability at low energies. Because of the finite size of the chain we cannot study the zero-energy limit; however, we expect the transmission to vanish at this limit, as implied by comparing the $N = 121$ and $N = 301$ data at low energies. We should also note that the results are practically independent of system size, at least in this lowest-branch approximation. Similar results are shown in Fig. 8 for the isotropic model at different potential strengths g, where, as expected, the transmission is suppressed with increasing potential strength. Furthermore, as in the free-spinon case, note the vanishing of the transmission at high energies, related to the zero-spinon velocity at the top of the energy dispersion.

As shown in Fig. 3, in an even chain there are two low-energy spinon branches. In Fig. 9 we find that there is a complementarity in transmission, as when $\mathcal{T}_{Q,Q}$ decreases, $\mathcal{T}_{Q,Q+\pi}$ increases. The sum of the two closely resembles the transmission of the one spinon in an odd chain. Furthermore, there is a strong size dependence of $\mathcal{T}_{Q,Q}$ which can probably

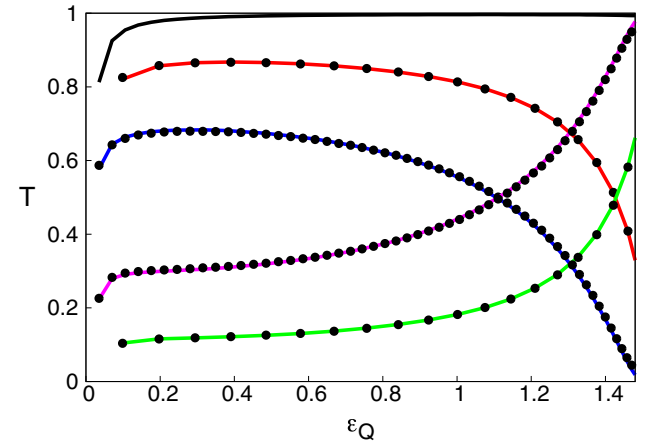

FIG. 9. $\mathcal{T}_{Q,Q}$ (red, $N = 100$; blue, $N = 280$) and $\mathcal{T}_{Q,Q+\pi}$ (green, $N = 100$; purple, $N = 280$) vs ε_Q for $g = 0.15$ and $\Delta = 1$. The sum $\mathcal{T}_{\rm tot} = \mathcal{T}_{Q,Q} + \mathcal{T}_{Q,Q+\pi}$ for $N = 280$ is indicated by the solid black line. The solid lines represent the analytical results, while the dots show the numerical data.

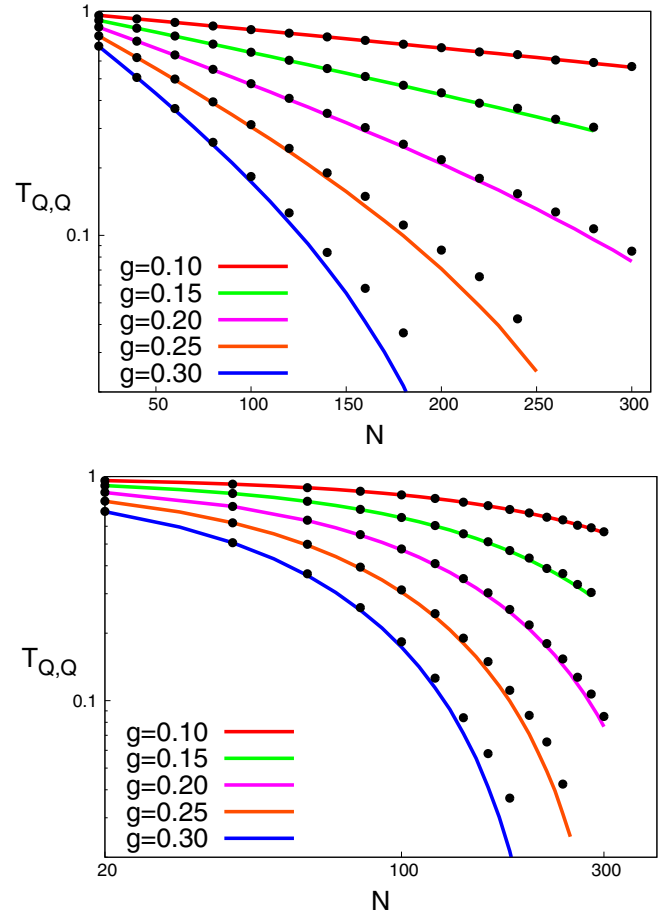

FIG. 10. $\log_{10}\mathcal{T}_{Q,Q}$ vs N (top) and $\log_{10}\mathcal{T}_{Q,Q}$ vs $\log_{10}N$ (bottom) for $V = gS^z_n$ for the isotropic model $\Delta = 1$ and energy $\varepsilon_Q = \frac{\pi}{2}\sin(2\pi/10) \simeq 0.92$. The solid lines represent the analytical approximation [19], while the dots represent the numerical data.

best be described as exponentially decreasing with N. This is argued in [19] and shown in Fig. 10, where for comparison a power law dependence is also plotted (not shown, there is a corresponding exponential increase of $\mathcal{T}_{Q,Q+\pi}$). The exponential dependence increases with Δ, as shown in Fig. 11, and with g (Fig. 10). However, the sum $\mathcal{T}_{Q,Q} + \mathcal{T}_{Q,Q+\pi}$ of transmission probabilities shows a weak size dependence and, of course, in the $\Delta = 0$ case coincides with the one spinon in an odd chain with no size dependence. In other words, we conjecture that in the thermodynamic limit an incoming spinon from the one branch is fully transmitted and reflected in the other branch. In this calculation we have again included as intermediate states only the two lower spinon branches. As discussed below, including all the two-spinon states only quantitatively changes this behavior. Another aspect of this transfer of transmission probability from the $\mathcal{T}_{Q,Q}$ to the $\mathcal{T}_{Q,Q+\pi}$ branch is shown in Fig. 12, where we see that $\mathcal{T}_{Q,Q+\pi}$ increases with potential strength.

Based on the integrable structure of the Heisenberg model, we can understand these results from first principles [19]. Resumming to all orders the most important on-shell matrix elements, $|Q\rangle \to |Q+\pi\rangle, |\pi - Q\rangle$, described in the previous section, we obtain a fairly good description of the

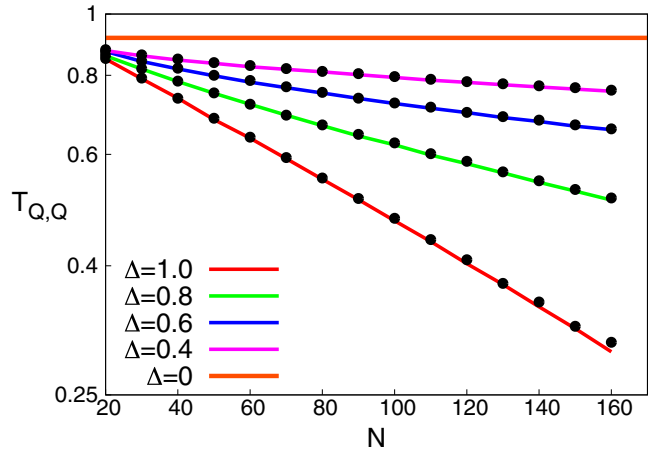

FIG. 11. $\log_{10}\mathcal{T}_{Q,Q}$ vs N for $V = gS^z_n$, $g = 0.2$ for constant energy $\varepsilon_Q/v_s = \sin(2\pi/10)$ and $\Delta = 0.4, 0.6, 0.8, 1.0$ The solid lines represent the analytical approximation [19], while the dots represent the numerical data. The horizontal line represents the $\Delta = 0$ case.

transmission probabilities (even quantitative in the weak-coupling limit). It is easily proved that these transitions result in a monotonically decreasing (increasing) transmission probability $\mathcal{T}_{Q,Q}(\mathcal{T}_{Q,\pi+Q})$ with spin chain length N. We expect this behavior to be generic in one-dimensional spin chains; simply, here, the integrability of the model allows us to explicitly evaluate the corresponding exponents.

By a numerical fit in Figs. 10 and 11 we find that a useful quantity for the description of the scattering process is $g_{\text{eff}} = gN^{1-\mathcal{Z}^2}$ and that for ε_Q not close to zero the transmission coefficient behaves as

$$\mathcal{T}_{Q,Q} \simeq e^{-a(g_{\text{eff}}/u_Q)^2}, \tag{15}$$

which holds for $g_{\text{eff}}/u_Q \ll 1$. Thus, for the isotropic Heisenberg model ($\gamma = 0,\ \Delta = 1$) which is the most experimentally relevant $\mathcal{T}_{Q,Q} \simeq e^{-a(g/u_Q)^2 N}$. Although this approach does not offer an analytical solution of the scattering problem, using the framework of integrability, we derived a connection between the transmission coefficients and $\theta_{zz} = 2\mathcal{Z}^2$, the critical exponent of the ground state's correlation function $\langle 0|s^z_1 s^z_{n+1}|0\rangle$

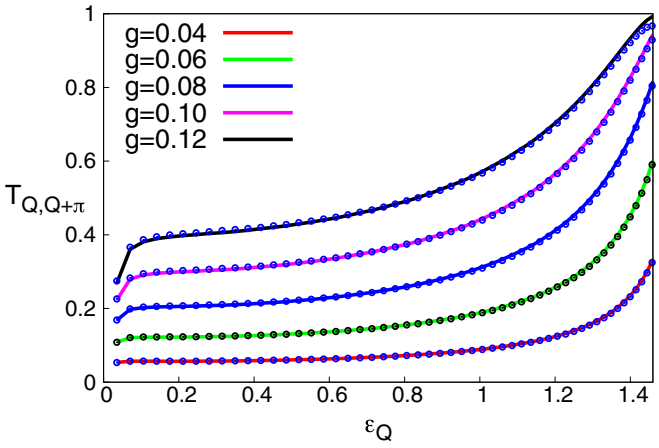

FIG. 12. $\mathcal{T}_{Q,Q+\pi}$ vs ε_Q as a function of g for $N = 280$. The solid lines are guides to the eye.

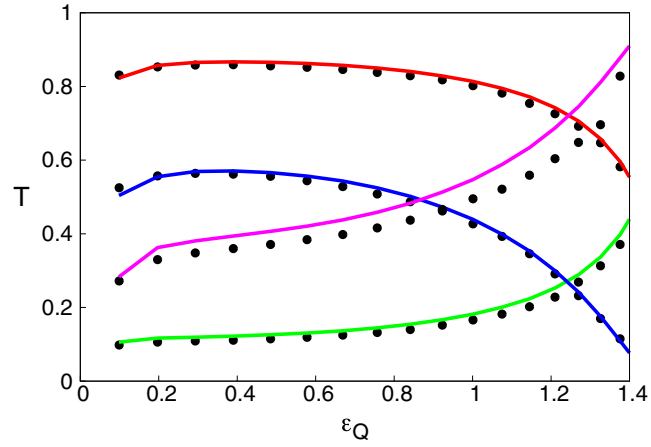

FIG. 13. $\mathcal{T}_{Q,Q}$ (red, $g = 0.1$; blue, $g = 0.2$) and $\mathcal{T}_{Q,Q+\pi}$ (green, $g = 0.1$; purple, $g = 0.2$) vs ε_Q for $N = 100$ and $\Delta = 1$. The solid lines are produced by including only the lower branch, while the dots represent the numerical data obtained by including the whole two-spinon continuum.

dominant oscillatory part. Predicted by conformal field theory and Bethe ansatz calculations [16,22], it offers a qualitative description of the scattering process.

Note that this approximation gives reasonable results even though we have performed a rough elimination of most of the intermediate matrix elements. On the other hand, from the specific form of the transmission probability of the free-spinon model we observe that the dominant behavior is given by the on-shell matrix elements and the rest of the matrix V serves as a correction, which justifies the reasoning for the above approximation. Of course, as we see in Fig. 10, it is a weak-coupling approximation, albeit a very good one, that becomes increasingly unreliable in the strong g coupling limit. Even more, in the strong coupling $g/u_Q \gg 1$ limit (e.g., $Q \to \pm\pi/2$) the numerical T-matrix approach we are using often does not converge at all.

Finally, to improve the lower-branch approximation we include all the two-spinon de Cloizeaux–Pearson [18] states, which forces us, however, to study rather small spin chains as the space of intermediate states increases as N^2. As shown in Figs. 13 and 14, the inclusion of the two-spinon states results in only quantitative differences with most of the effect coming from the $\mathcal{T}_{Q,Q+\pi}$ transition. We estimate the $N \to +\infty$ extrapolated value of $\mathcal{T}_{\text{tot}}$ to be reduced by about 30% from the value of the lower branch data. We should note, however, that the two-spinon continuum data become increasingly sensitive with system size to details of the calculation, e.g., separation of the real and imaginary parts in the T-matrix numerical evaluation.

Comparing the even- and odd-site cases, we find an interesting topological effect. In the odd chains, in our one-spinon study where the spectrum is twofold degenerate, we find a rather regular behavior of scattering coefficients. In the even chains, due to the topological two-spinon constraint, we have a fourfold-degenerate spectrum that, together with the singular π transition, implies a transfer of transmission probability between the two spinon branches. Thus, in the

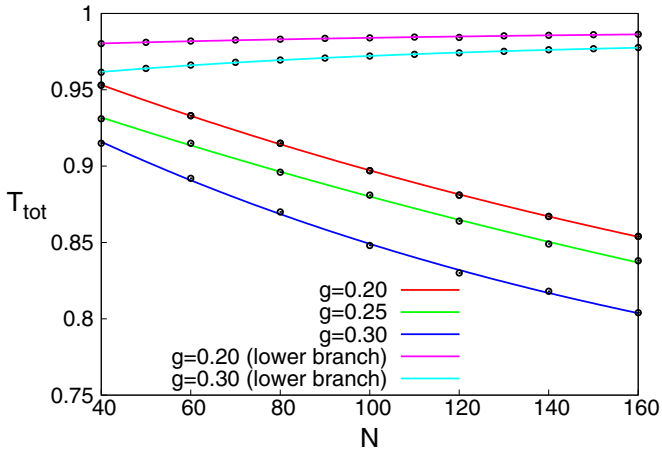

FIG. 14. $\mathcal{T}_{\rm tot}$ versus N for the $V = gS^z_n$ potential $\Delta = 1$ and $\varepsilon_Q \simeq 0.923$ including the two-spinon continuum along the lower-branch data. The dots represent the numerical data, while the solid lines represent the fitted curve $\mathcal{T}_{\rm tot} = A\exp(-Bf^z(Q)g^2N/u_Q^2) + C$.

spinon scattering, we have an interplay of the topological character and the singular matrix elements of a critical system.

C. Spin-phonon potential

The spin-phonon interaction is described by a one-link potential of the form

$$V = g(S^-_n S^+_{n+1} + S^+_n S^-_{n+1}). \tag{16}$$

In Fig. 15 the numerical calculation for an even-site chain shows that $\mathcal{T}_{Q,Q} \to 0$ as N increases. Like in the previous case, we obtain an approximate analytical result by using the dominant matrix elements that were described in the previous section. In particular, the monotonicity of the scaling factors implies that the transmission and reflection coefficients will be scale invariant for $\Delta = 0$, while on the contrary, for $0 < \Delta \leqslant 1$, $\mathcal{T}_{Q,Q} \to 0$ as N increases. Moreover, the relation of the scattering coefficients to the spinon energy ε_Q is very similar

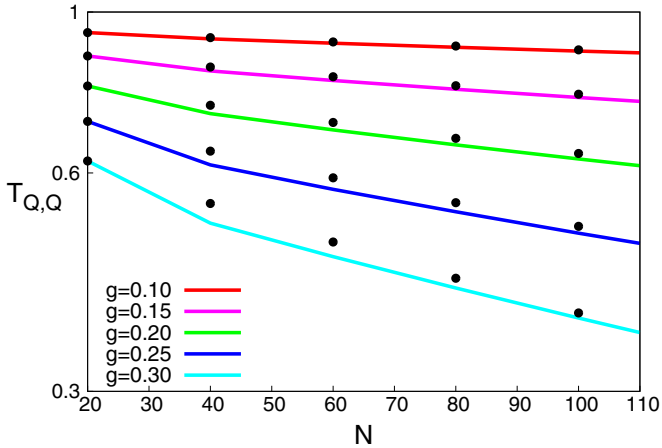

FIG. 15. $\log_{10}\mathcal{T}_{Q,Q}$ vs N for a one-link spin-phonon potential V, $\varepsilon_Q \simeq 0.92$, and $g = 0.1, 0.15, 0.2, 0.25, 0.3$. Solid lines are predictions based on the dominant matrix elements [19].

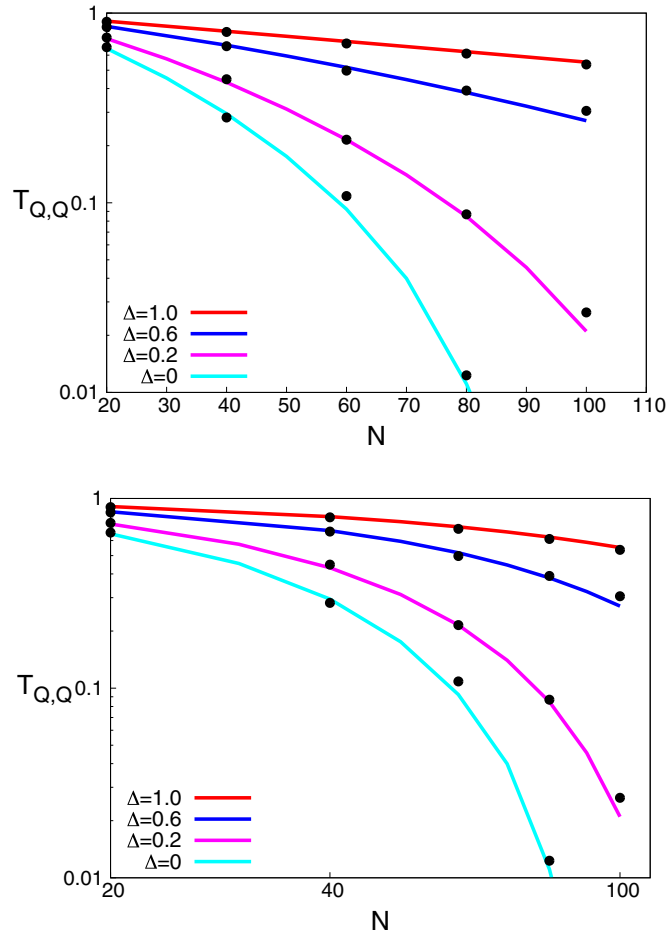

FIG. 16. $\log_{10}\mathcal{T}_{Q,Q}$ vs system size N (top) and $\log_{10}\mathcal{T}_{Q,Q}$ vs system size $\log_{10}N$ for a one-site transverse potential $V = gS^x_n$, $g = 0.2$, $\varepsilon_Q = v_s\sin(\frac{2\pi}{10})$, and $\Delta = 1, 0.6, 0.2, 0.0$. Solid lines are the prediction considering the dominant matrix elements [19].

to that of a longitudinal magnetic potential, as was depicted in Fig. 9.

D. Transverse potential

We now turn to a transverse magnetic potential, $V = gS^x_n$. The main difference of this potential from the two previous ones we studied is that it acts nontrivially only between states with $\Delta S^z = \pm 1$. We will restrict ourselves to transitions between the $S^z = 1$ and $S^z = 2$ magnetization sectors.

Figure 16 shows that like in the previous cases, for an even-site chain $\mathcal{T}_{Q,Q} \to 0$ as N increases. Again, the dependence is probably best described as exponential, as argued in [19] and by comparison with a power law one. However, this time we find that this holds also for $\Delta = 0$, and in fact the scattering increases as Δ decreases, which is the opposite of what happened in the previous cases. Again, we can obtain a qualitative explanation of this behavior by using the fact [25,26] that the dominant matrix element approximately scales as $\theta_{-+} = \frac{1}{2\mathcal{Z}^2} \simeq \frac{\pi-\gamma}{\pi}$, which is the dominant critical exponent of the ground-state correlation $\langle 0|\sigma^-_1\sigma^+_{n+1}|0\rangle$. By resummation [19] and the monotonicity of the critical exponents with respect to Δ one can argue that $\mathcal{T}_{Q,Q} \to 0$ for $0 < \Delta \leqslant 1$. Nevertheless,

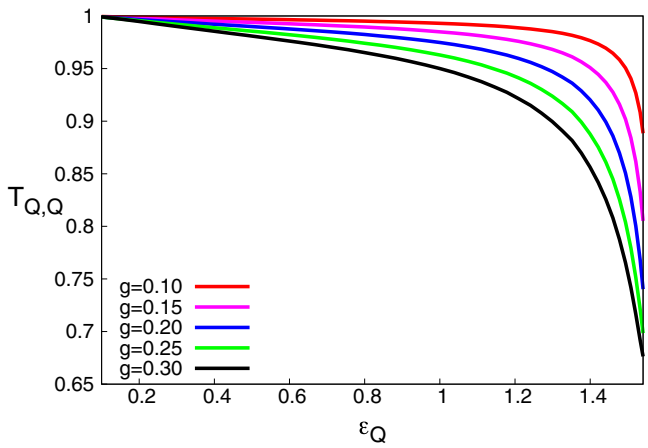

FIG. 17. $\mathcal{T}_{Q,Q}$ vs spinon energy ε_Q for a potential $V = g(S^z_n + S^z_{n+1})$, $N = 201$.

a full-scale analysis of the matrix elements should be done in order to give a definite answer. Similar to what we did in the previous cases, by defining $g_{\text{eff}} \equiv gN^{1-\frac{1}{4Z^2}}$, implying $g_{\text{eff}} = g\sqrt{N}$ for $\Delta = 1$ (isotropic model) and $g_{\text{eff}} = gN^{3/4}$ for $\Delta = 0$ (XY model), we conclude that

$$\mathcal{T}_{Q,Q} \simeq e^{-f^x(Q)(g_{\text{eff}}/u_Q)^2} \tag{17}$$

in the region $g_{\text{eff}}/[4u_Q^2/f^x(Q)] \ll 1$, a behavior which agrees well with the numerical data.

E. Extended potential

Finally, we consider the spinon scattering from an extended potential

$$V_{\text{ext}} = \sum_{n=1}^{m} g_n V_n. \tag{18}$$

Using the numerical procedure presented earlier, we can calculate the transmission probability for an arbitrary potential profile $\{g_n\}$ in the two-spinon continuum approximation. We start with the scattering of a spinon in an odd chain by a two-site longitudinal potential, a case analogous to Fig. 7 for an on-site potential. In Fig. 17 we see a remarkable difference at low energies where there is complete transmission. This situation is consistent with the well-known "cutting" and "healing" [30,31] effect in one-dimensional correlated systems and spin chains, where one weak link is cutting a chain at low energies while two weak links are healed. This effect leads to a finite conductance with a power law dependence on the temperature due to thermal effects.

Here, we can understand the results of extended potentials by considering the "diffraction" relation (12). For an $m = 2$ longitudinal potential in an odd chain, at low energies $Q \to 0$, the $q = \pi - 2Q$ scattering matrix element vanishes, leading to total transmission. Following the same argument, we also find that for an even chain with an $m = 2$ longitudinal potential the transfer of transmission probability from $\mathcal{T}_{Q,Q}$ to $\mathcal{T}_{Q,Q+\pi}$ found in Fig. 7 is now totally suppressed as the $q = \pi$ matrix element vanishes. Following the same line of resummation of dominant matrix elements and taking into account the corresponding diffraction factor allow us to understand the transmission by extended potentials.

IV. CONCLUSIONS

Using the Bethe ansatz method and the T-matrix approach, we have studied the scattering of a spinon from prototype potentials. Three main features emerged from this study; first, we are considering a quantum many-body problem, so in principle outgoing states with the creation of spinons or "electron-hole" pairs are possible, although we expect from the scattering matrix elements that these processes have lower probability. We have limited our study to outgoing states with the same number of spinons as the incoming state. Second, we can qualitatively account for the transmission probabilities by resumming the dominant scattering elements. Their dependence on the size of the spin chain is given by the critical exponents characterizing the anisotropic Heisenberg model. Thus, we linked the scattering to the critical properties of this integrable model, and we evaluated them using the Bethe ansatz method. Whether including all intermediate states $O(2^N)$ would qualitatively change the present picture is an open, technically very difficult, question. Third, we have found an intriguing topological effect as, in an even chain, there is complete transfer of the incoming spinon transmission probability from the one branch of the dispersion to the other branch. At the moment, in a macroscopic open chain the role of this odd-even effect is ambiguous. Further study is necessary to clarify it, presumably including further outgoing states, e.g., three-spinon states in odd chains. Note that several experimental and theoretical studies [29] have addressed the physical effect of even vs odd chain length in the thermodynamic properties of finite-size chains.

Along the lines of dominant matrix elements, we analyzed a basic difference in the scattering coefficients of longitudinal and weak-link potentials from those of a transverse potential. We also discussed extended potentials where we attributed a drastic dependence of scattering coefficients on the potential extent to a geometric diffraction factor and dominant scattering matrix elements. These results are consistent with previous studies on cutting and healing in 1D correlated systems [30–32].

Considering experiment, we studied the problem of a spinon excited above the ground state and scattering from a potential. Although we have not addressed any particular experiment, our study should provide key elements in the interpretation of far-out-of-equilibrium experiments as well as thermal transport ones, for instance, zero-temperature tunneling studied by a "Landauer"-type approach or spinon transport probed, e.g., by terahertz two-dimensional coherent spectroscopy [33] experiments.

ACKNOWLEDGMENTS

This work was supported by European Union Program No. FP7-REGPOT-2012-2013-1 under Grant No. 316165, the Deutsche Forschungsgemeinschaft through Grant No. HE3439/13, the Alexander von Humboldt Foundation, the Hellenic Foundation for Research and Innovation (HFRI),

and the General Secretariat for Research and Technology (GSRT), under HFRI PhD Fellowship Grant No. KA4819. A.P. acknowledges valuable discussions with P. Lambropoulos, N. Kitanine, and J.S. Caux. X.Z. acknowledges fruitful discussions with H. Tsunetsugu, A. Klümper, T. Tomaras, C. Hess, B. Büchner, A. Chernyshev, and S. White and the hospitality of the Institute for Solid State Physics at the University of Tokyo and the University of California, Irvine.

[1] C. Hess, Eur. Phys. J. Spec. Top. **151**, 73 (2007); Physics Reports **811**, 1 (2019).
[2] X. Zotos, F. Naef, and P. Prelovšek, Phys. Rev. B **55**, 11029 (1997).
[3] A. Klümper and K. Sakai, J. Phys. A **35**, 2173 (2002).
[4] E. Shimshoni, N. Andrei, and A. Rosch, Phys. Rev. B **68**, 104401 (2003).
[5] K. Louis, P. Prelovšek, and X. Zotos, Phys. Rev. B **74**, 235118 (2006).
[6] A. L. Chernyshev and A. V. Rozhkov, Phys. Rev. Lett. **116**, 017204 (2016).
[7] X. Zotos, J. Stat. Mech. (2017) 103101.
[8] G. E. W Bauer, E. Saitoh, and B. J. van Wees, Nat. Mater. **11**, 391 (2012).
[9] L. J. Cornelissen, J. Liu, R. A. Duine, J. Ben Youssef and B. J. van Wees, Nat. Phys. **11**, 1022 (2015), and references therein in this rapidly expanding field.
[10] D. Hirobe, M. Sato, T. Kawamata, Y. Shiomi, K. Uchida, R. Iguchi, Y. Koike, S. Maekawa, and E. Saitoh, Nat. Phys. **13**, 30 (2017); J. Appl. Phys. **123**, 123903 (2018).
[11] M. Takahashi, *Thermodynamics of One-Dimensional Solvable Models* (Cambridge University Press, Cambridge, 2005).
[12] K. Louis and C. Gros, Phys. Rev. B **67**, 224410 (2003).
[13] K. Sakai and A. Klümper, J. Phys. Soc. Jpn. Suppl. **74**, 196 (2005).
[14] C. Psaroudaki and X. Zotos, J. Stat. Mech. (2016) 063103.
[15] L. D. Faddeev and L. A. Takhtajan, Phys. Lett. **85A**, 375 (1981).
[16] N. Kitanine, J. M. Maillet, and V. Terras, Nucl. Phys. B **554**, 647 (1999).
[17] J. S. Caux, R. Hagemans, and J. M. Maillet, J. Stat. Mech. (2005) P09003.
[18] J. des Cloizeaux and J. J. Pearson, Phys. Rev. **128**, 2131 (1962).
[19] See Supplemental Material at http://link.aps.org/supplemental/10.1103/PhysRevB.100.134401 for further details on the dominant matrix elements and scattering theory calculations (see also Refs. [34,35,36]).
[20] For our convention for S^z_q, $|\langle Q+q|S^z_q|Q\rangle|^2 = N|\langle Q+q|S^z_n|Q\rangle|^2$.
[21] D. Biegel, M. Karbach, G. Müller, and K. Wiele, Phys. Rev. B **69**, 174404 (2004).
[22] V. E. Korepin, Teor. Mat. Fiz. **41**, 169 (1979) [Teor. Math. Phys. **41**, 953 (1979)].
[23] N. M. Bogolyubov, A. G. Izergin, and V. E. Korepin, Nucl. Phys. B **275**, 687 (1986).
[24] M. Dugave, F. Göhmann, and K. K. Kozlowski, SIGMA **10**, 043 (2014).
[25] N. Kitanine, K. K. Kozlowski, J. M. Maillet, N. A. Slavnov, and V. Terras, J. Stat Mech. (2011) P05028.
[26] N. Kitanine, K. K. Kozlowski, J. M. Maillet, N. A. Slavnov, and V. Terras, J. Stat. Mech. (2014) P05011.
[27] T. R. Robinson, Am. J. Phys. **80**, 141 (2012).
[28] V. J. Emery, in *Highly Conducting One-Dimensional Solids*, edited by J. T. Devresee, R. E. Evrard, and V. E. van Doren (Plenum, New York, 1979), pp. 247–303.
[29] J. Sirker, S. Fujimoto, N. Laflorencie, S. Eggert, and I. Affleck, J. Stat. Mech. (2008) P02015, and references therein.
[30] C. L. Kane and M. P. A. Fisher, Phys. Rev. Lett. **68**, 1220 (1992); Phys. Rev. B **46**, 15233 (1992).
[31] S. Eggert and I. Affleck, Phys. Rev. B **46**, 10866 (1992).
[32] A. Metavitsiadis, X. Zotos, O. S. Barišić, and P. Prelovšek, Phys. Rev. B **81**, 205101 (2010).
[33] Y. Wan and N. P. Armitage, Phys. Rev. Lett. **122**, 257401 (2019).
[34] H. Bethe, Z. Phys. **71**, 205 (1931).
[35] V. E. Korepin, N. M. Bogoliubov, and A. G. Izergin, *Quantum Inverse Scattering Method and Correlation Functions* (Cambridge University Press, Cambridge, 2010).
[36] E. Merzbacher, *Quantum Mechanics* (John Wiley & Sons, New York, 1998).